Food Chemistry: X 24 (2024) 101836

Contents lists available at ScienceDirect

Food Chemistry: X

journal homepage: www.sciencedirect.com/journal/food-chemistry-x

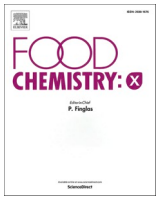

Preparation and characterization of lactoferrin-polyphenol conjugate with stabilizing effects on fish oil high internal phase Pickering emulsions

Ying Sun [a], Mantong Zhao [a], Zhongyuan Liu [a], Haohao Shi [a], Xueying Zhang [a], Yongqiang Zhao [b], Zhenhua Ma [b], Gang Yu [b], Guanghua Xia [a,c,*], Xuanri Shen [d]

[a] Hainan Engineering Research Center of Aquatic Resources Efficient Utilization in South China Sea, Key Laboratory of Food Nutrition and Functional Food of Hainan Province, Key Laboratory of Seafood Processing of Haikou, College of Food Science and Technology, Hainan University, Hainan 570228, China.
[b] Sanya Tropical Fisheries Research Institute, Sanya 572018, China
[c] Collaborative Innovation Center of Provincial and Ministerial Co-Construction for Marine Food Deep Processing, Dalian Polytechnic University, Dalian 116034, China.
[d] College of Food Science and Technology, Hainan Tropical Ocean University, Sanya 572022, China.

ARTICLE INFO

Keywords:
Lactoferrin
Polyphenol
Covalent complex
High internal phase Pickering emulsions
Stability

ABSTRACT

The combination of protein and polyphenol is an effective approach to improve the stability of protein emulsions. The lactoferrin (LF)-(−)-epigallocatechin-3-gallate (EGCG) covalent complex (LF-EGCG) was first prepared by alkali-induced reaction, then the structure and physicochemical properties between LF-EGCG and non-covalent complex (LF + EGCG) were compared, and finally the stability of complexes to fish oil high internal Pickering emulsions (HIPPEs) was tested. Results showed that LF-EGCG had stronger antioxidant activity, higher thermal stability, and better surface wettability than LF + EGCG. Meanwhile, the complexes showed no cytotoxicity within the tested concentration range (12.5–200 μg/mL). The HIPPEs stabilized with LF-EGCG possessed smaller droplet size, higher ζ-potential, and more uniform oil/water proton distribution. Covalent treatment also enhanced the storage, thermal, freeze-thaw and physical stability of LF HIPPEs. Furthermore, due to the higher antioxidant activity and denser microstructure, LF-EGCG HIPPE can more effectively inhibit the oxidation of fish oil.

1. Introduction

High internal phase Pickering emulsions (HIPPEs) are the emulsions stabilized by solid particles with an internal phase volume fraction exceeding 74 % (Zhang, Fan, Liu, & Li, 2023). In terms of resistance to Ostwald ripening, phase separation, and coalescence, HIPPEs are more stable than conventional emulsions (Song et al., 2023). However, the inedibility of some inorganic particles limits their application in food field. Research has shown that compared with inorganic particles, HIPPEs stabilized with food-grade solid particles such as proteins and polysaccharides are safe, non-toxic, edible, and biocompatible (Xu, Tang, Liu, & Liu, 2018).

Lactoferrin (LF), an iron-bound glycoprotein, is composed of two homologous globular lobes connected by a α-helical polypeptide (Liu, Sun, Yang, Yuan, & Gao, 2015). It has many physiological activities, such as antibacterial, antioxidant, and immune regulation (Liu, Wang, Sun, McClements, & Gao, 2016). To the best of our knowledge, there have been no reports about HIPPEs stabilized with LF. Due to insufficient surface wettability, single protein particles are often unstable as emulsifiers. The introduce of polyphenols can further enhance the oil-water interface film by improving wettability of protein particles (Zou, Guo, Yin, Wang, & Yang, 2015). (−)-epigallocatechin-3-gallate (EGCG) is a green tea polyphenol with strong antioxidant and antibacterial properties. It can form complexes with proteins via non-covalent and covalent interactions, which can enhance the stability of emulsions through improving their interfacial and antioxidant properties (Tong et al., 2021). Compared with non-covalent complexes, covalent complexes were more resistant to environmental stresses, and had higher potential to inhibit lipid oxidation (Feng, Cai, Wang, Li, & Liu, 2018). In the previous report, Wei, Yang, Fan, Yuan, and Gao (2015) confirmed that milk protein-polyphenol covalent complexes had higher denaturation temperatures, antioxidant activity, and interfacial adsorption

* Corresponding author at: Hainan Engineering Research Center of Aquatic Resources Efficient Utilization in South China Sea, Key Laboratory of Food Nutrition and Functional Food of Hainan Province, Key Laboratory of Seafood Processing of Haikou, College of Food Science and Technology, Hainan University, Hainan 570228, China.
E-mail address: xiaguanghua@hainanu.edu.cn (G. Xia).

https://doi.org/10.1016/j.fochx.2024.101836
Received 14 July 2024; Received in revised form 29 August 2024; Accepted 12 September 2024
Available online 17 September 2024

behavior than those of non-covalent complexes. Ovalbumin-catechin conjugates had higher storage stability, lipid oxidation stability, and interfacial accumulation (Feng et al., 2018).

Fish oil, the main source of omega-3 polyunsaturated fatty acids, has anti-inflammatory, brain-strengthening and immunomodulatory effects, so it was selected as the oil phase to improve the nutritional value of emulsions (Zhao et al., 2021). In this study, we aimed to prepare lactoferrin-EGCG covalent complex by alkali treatment to stabilize fish oil HIPPEs, and then compared the structural and functional properties of covalent and non-covalent complexes. Here, we hypothesized the covalent modification could enhance the emulsification of lactoferrin and the lipid oxidation stability of HIPPEs. We characterized the structural and physicochemical properties of complexes, and explored the particle size, ζ-potential, microstructure, microrheology, water-oil distribution, lipid oxidation and environmental stress stability of HIPPEs. This study provided a theory basis for emulsion-based delivery of healthy lipids and bioactive substances.

2. Materials and methods

2.1. Materials

Lactoferrin (LF, purity ≥96.26 %) was bought from Westland Milk Products Co. (Hokitika, New Zealand). EGCG (purity ≥98 %) was obtained from Meryer Biochemical Technology Co., Ltd. (Shanghai, China). Fish oil, DTNB (5,5'-Dithiobis-(2-nitrobenzoic acid), and orthophthaldialdehyde (OPA) were purchased from Shanghai Macklin Biochemical Technology Co., Ltd. (Shanghai, China). DPPH was purchased from Aladdin Biochemical Technology Co., Ltd. (Shanghai, China). ABTS free radical scavenging ability test kit and LPO content assay kit were purchased from Solarbio Co., Ltd. (Beijing, China), and the MDA content assay kit was obtained from Suzhou Grace Biotechnology Co., Ltd. (Suzhou, China). Other reagents were of analytical grade.

2.2. Fabrication of lactoferrin-EGCG complexes

The covalent complex was prepared by alkali treatment (Liu, Sun, Wang, Yuan, & Gao, 2015). LF solution (1 % (*w/v*), pH 9.0) was prepared and mixed with 0.2 % (w/v) EGCG aqueous solution of the same volume, then the pH was adjusted to 9.0 using 1 mol/L HCl and 1 mol/L NaOH solutions. The mixture was exposed to the air and stirred for 24 h at 25 °C. After that, it was dialyzed (MWCO: 8000–14,000 Da) at 4 °C for 48 h. The dialysate was freeze-dried (Christ Epsilon 2-10D, Marin Christ Co., Osterode, Germany) and the solid was named LF-EGCG.

The non-covalent mixture was used as control. Equal volumes of LF solution and EGCG solution were mixed and sealed at 25 °C for 24 h without adjusting the pH, the resulting solid was LF + EGCG.

2.3. Binding amount of EGCG and LF

In brief, 2 % (*w/v*) of protein solution (1 mL) and 0.2 N of Folin-Ciocalteu reagent (5 mL) were mixed and placed in the dark for 5 min. Then 7.5 % (*w/v*) of Na_2CO_3 solution (2 mL) was added and placed in the dark for 2 h. The mixture was detected at 760 nm using an UV–visible spectrophotometer (UV-1800, Shimadzu Co., Ltd., Kyoto, Japan). The final result was expressed as mg EGCG equivalent per g sample (Feng et al., 2018).

2.4. Measurement of free amino group

Briefly, OPA (40 mg) was dissolved in 1 mL of methanol, then the solution was blended with 2.5 mL of 20 % (w/v) SDS solution, 25 mL of 0.1 mol/L borax solution, and 100 μL β-mercaptoethanol. The mixture was adjusted to 50 mL using deionized water to prepare OPA reagent. Each 200 μL of protein solution was blended with 4 mL of OPA reagent and incubated at 35 °C for 2 min. The absorbance of samples was determined at 340 nm (Liu, Sun, Wang, et al., 2015).

2.5. Determination of sulfhydryl group

DTNB (4 mg) was dissolved in 1 mL of Tris-glycine buffer to prepare Ellman reagent. The sample (15 mg) was dissolved in Tris-glycine buffer, then it was mixed with 50 μL of Ellman reagent. After standing at 25 °C for 1 h, the mixture was detected at 412 nm. The content of sulfhydryl group was calculated according to the equation: $\mathrm{SH}\ (\mu\mathrm{mol/g}) = 73.53 \times A_{412}/C$, here C was the sample concentration (mg/mL) (Beveridge, Toma, & Nakai, 1974).

2.6. Matrix-assisted laser desorption/ionization time-of-flight mass spectrometry (MALDI-TOF-MS)

MALDI-TOF-MS (Ultraflextreme MALDI-TOF/TOF mass spectrometer, Bruker Daltonic Inc., Massachusetts, USA) was applied to characterize the molecular weight of samples. The 0.5 μL of protein solution (1 mg/mL) was injected to the plate, then covered with 0.5 μL of saturated α-Cyano-4-hydroxycinnamic acid. Parameter settings: reflector mode, acceleration voltage of 20 kV, effective flight path of 200 cm.

2.7. Circular dichroism (CD)

The protein particles were dispersed in 10 mmol/L PBS (pH 7.0) and detected at 190–260 nm and 250–320 nm using a circular dichroism spectrometer (MOS-500, Biologic Co., Ltd., Grenoble, France).

2.8. Fourier transform infrared (FTIR) spectroscopy

The protein and potassium bromide (1:99) were mixed and ground a tablet. The spectra were collected at 400–4000 cm^{-1} for 32 scans with a resolution of 4 cm^{-1} using a FTIR spectrometer (Nicolet 5700, Thermo Nicolet Co., Waltham, USA).

2.9. Fluorescence spectroscopy

The sample solution (0.5 mg/mL) was scanned by the fluorescence spectrophotometer (FLS1000, Edinburgh Instruments Co., The Towns of Edinburgh, Britain). The excitation wavelength (E_x) was 280 nm and the emission wavelength (E_m) range was 300–500 nm. The excitation and emission slit width were both 5.0 nm, and the scan rate was 1200 nm/min. The E_x and E_x ranges of three-dimensional fluorescence spectra were 200–350 nm and 200–500 nm, respectively. Each spectrum was recorded at every 5 nm increase at a scanning rate of 30,000 nm/min. (Feng et al., 2023).

2.10. Differential scanning calorimetry (DSC)

The sample (6 mg) was put into the aluminum pan and sealed, then it was heated from 30 °C to 180 °C at a speed of 10 °C/min using the differential scanning calorimeter (DSC7000, Hitachi Co., Tokyo, Japan) (Wan et al., 2023).

2.11. Antioxidant activities

2.11.1. DPPH scavenging activity

The 1 mL of protein solution (0.5 mg/mL) was mixed with 3 mL of DPPH solution (0.4 mmol/L). The mixture was incubated at 25 °C in the dark for 30 min and detected at 517 nm. DPPH scavenging activity was calculated as follows:

$$\text{DPPH scavenging activity} = (1 - A_s/A_c) \times 100 \quad (1)$$

where, A_s and A_c were the absorbance of the sample and control at 517

nm, respectively.

2.11.2. ABTS scavenging activity

The ABTS radical scavenging activity of complexes was detected by an ABTS free radical scavenging ability test kit and calculated as Eq. (2):

$$\text{ABTS scavenging activity} = [1 - (A_1 - A_2)/A_0] \times 100 \quad (2)$$

here, A_0, A_1, and A_2 were the absorbance of the control, sample, and sample only, respectively.

2.11.3. Reducing power

Briefly, 2 mL of protein solution was blended with 1 mL of $K_3[Fe(CN)_6]$ solution (1 %, m/v). The mixture was incubated at 50 °C for 20 min. Then, 1 mL of $C_2HCl_3O_2$ solution (10 %, *w/v*) was added and blended thoroughly. Absorbed 1 mL of the above solution, then added 3 mL of deionized water and 0.4 mL of $FeCl_3$ solution (0.1 %, w/v). The system was reacted for 5 min at 25 °C and detected at 700 nm. The reducing capacity of sample was compared with that of V_c, and the final result was represented as V_c equivalent (V_c equivalent/g dry base) (Yıldırım, Mavi, & Kara, 2001; Zhang, Fan, et al., 2023).

2.12. Cytotoxicity

The cytotoxicity of protein solution (0–200 μg/mL) was assessed by the 3-(4,5-dimethylthiazol-2-yl)-2,5-diphenyltetrazolium bromide (MTT) method (Liu et al., 2022). The trypsin digestive solution (1 mL) was added to Caco-2 cells at the logarithmic growth stage for 3 min, then the cells were diluted to 1×10^4 cells/well. The diluted cells were added to a 96-well plate and incubated in an incubator (5 % CO_2, 37 °C) for 24 h. After removing the medium, 100 μL of fresh culture medium with different concentrations (0, 12.5, 25, 50, 100, and 200 μg/mL) of protein samples was added to each well, and each group had 10 parallels. The culture mediums were continued to be cultured at 5 % CO_2, 37 °C for 24 h. After culturing, added 100 μL of MTT reagent (0.5 %, *w/v*) to each well and continued to culture for 4 h. Then, 100 μL of DMSO was added to each well. This system was left for 10 min to dissolve crystals, and the sample absorbance (A_{sample}) was measured at 560 nm, the absorbance of control group was $A_{control}$. The cell survival rate was calculated as Eq. (4):

$$\text{Cell survival rate } (\%) = A_{sample}/A_{control} \times 100 \quad (4)$$

where, A_{sample} and $A_{control}$ were the absorbance of sample and control at 560 nm, respectively.

2.13. Particle size and ζ-potential

The particle size and ζ-potential of samples were determined using a laser particle size analyzer (Zetasizer nano ZS90, Malvern Instruments Co., Worcestershire, UK). All samples were diluted to 0.1 % (*w/v*) and determined 3 times at 25 °C.

2.14. Atomic force microscopy (AFM)

The microstructure of samples was characterized by an AFM (MultiMode8, Bruker Co., Berlin, Germany) in a tapping mode. The captured 2D, 3D images and average roughness (R_q) values were analyzed by NanoScope_Analysis V2.0 software (Zhang, Wang, Huang, & Xu, 2024).

2.15. Three-phase contact angle ($\theta_{o/w}$)

The protein particles were pressed into a tablet and immersed in a fish oil bath. After dropping 2 μL of deionized water onto the tablet and equilibrating for 5 min, the $\theta_{o/w}$ was measured using a video optical contact anglemeter (OCA 25, Dataphysics Instruments Co., Stuttgart, Germany) (Wang et al., 2016).

2.16. Preparation of HIPPEs

The emulsions were stabilized with protein particles at different concentrations (0.3, 0.6, 0.9, 1.2, and 1.5 %, w/v). All emulsions were prepared by combining protein solution (20 %, *v*/v) and fish oil (80 %, v/v). The mixture was sheared at 10000 rpm for 3 min by a blender (Ultra Turrax T18, IKA Co., Baden-Württemberg, Germany).

2.17. Droplet size and ζ-potential

The droplet size of emulsions was measured through a laser diffraction particle size analyzer (Mastersizer 3000, Malvern Instruments Co., Ltd., Worcestershire, UK), and the ζ-potential of emulsions was detected by Zetasizer nano ZS90. All samples were diluted to 0.1 % (*w/v*) and determined 3 times at 25 °C.

2.18. Confocal laser scanning microscopy (CLSM)

The microstructure of HIPPEs was monitored by a CLSM (LMS800, Carl Zeiss Co., Jena, Germany). The oil phase and water phase were stained with Nile Red (1 mg/mL) and FITC (1 mg/mL), respectively. The HIPPEs were observed using a 40 × objective at different excitation wavelengths (488 nm and 525 nm) (Ma, Zou, McClements, & Liu, 2020).

2.19. Low-field NMR (LF-NMR) and magnetic resonance imaging (MRI)

The relaxation time T_2 distribution and MRI of HIPPEs were determined by the LF-NMR analyzer (NM120-040H-I, Niumag Analytical Instrument Co., Ltd., Suzhou, China). CPMG sequence was selected with RFD = 0.08 ms, TE = 1 ms, TW = 1000 ms, NECH = 8000, and NS = 4.

2.20. Lipid oxidation

Primary lipid oxidation product (lipid peroxide, LPO) and secondary lipid oxidation product (malondialdehyde, MDA) in HIPPEs were monitored to assess the lipid oxidative stabilities. Briefly, 10 g of HIPPE or fish oil was added to the sample bottle and stored at 50 °C for 15 days to accelerate the oil oxidation (Zhao et al., 2021). The contents of LPO and MDA in samples were measured by the LPO and MDA content assay kit every 3 days.

2.21. Stability evaluation of HIPPEs

2.21.1. Storage stability

HIPPEs were stored at 4 °C for 60 days. The microstructure, ζ-potential, and physical stability of HIPPEs were measured to assess the stability of the HIPPEs.

2.21.2. Thermal stability

The HIPPEs were heated at 40 °C for 30 min and then at 90 °C for 30 min. After cooling to 25 °C, the microstructure, ζ-potential, and physical stability of HIPPEs were determined to evaluate the effect of thermal treatment on the stability of HIPPEs.

2.21.3. Freeze-thaw stability

After thermal stability, HIPPEs were frozen at −20 °C for 24 h and then left at room temperature for 2 h (Wang et al., 2024a). The microstructure, ζ-potential, and physical stability of HIPPEs were determined to assess the freeze-thaw stability.

2.21.4. Physical stability

The transmission curves of the length and position of HIPPEs varying with centrifugation time were recorded using a stability analyzer (LUMiSizer 651, LUM GmbH Instruments Co., Ltd., Berlin, Germany).

The test temperature was 25 °C, the centrifugation speed was 4000 rpm, and the image capture time interval was 20 s (Feng, Wang, Wang, Xia, & Huang, 2021).

2.22. Diffusive wave spectroscopy (DWS) microrheology

The microrheological behavior of HIPPEs were measured by a microrheometer (Rheolaser Master, Formulaction Co., Toulouse, France) based on the report of Zhang et al. (2023). The freshly prepared emulsion was added to the sample bottle and analyzed for 12 h at 25 °C. Then the mean square displacement (MSD), solid-liquid balance (SLB), elasticity index (EI), macroscopic viscosity index (MVI), and fluidity index (FI) of the HIPPEs were analyzed and calculated.

2.23. Statistical analysis

All experiments of protein particles and emulsions were repeated 3 times. The results were analyzed using SPSS 23.0 and Origin 2021. One-way analysis of variance (ANOVA) was utilized to analyze the obvious variance among different groups ($p < 0.05$). The final result was mean values ± standard deviations.

3. Results and discussions

3.1. Characterization of complexes

3.1.1. Amount of EGCG bound to LF

Under alkaline and oxygen conditions, the ortho-hydroxyl groups of polyphenols are oxidized to o-quinone, which can react with the nucleophilic groups (amino and sulfhydryl) of proteins to form covalent C—N and C—S bonds (Liu, Sun, Wang, et al., 2015). As illustrated in Table S1, the total phenolic contents of LF-EGCG and LF + EGCG were 184.65 and 54.90 mg/g, respectively. It can be inferred that the covalent modification had stronger EGCG binding affinity, which corresponded to the previous report (Wei et al., 2015).

3.1.2. Free amino group and sulfhydryl group

The content of free amino group in samples reflected the relevant information of lysine side chains (Wei et al., 2015). In Table S1, the content of free amino group in LF-EGCG was markedly decreased compared with LF ($p < 0.05$). Similarly, Liu, Sun, Wang, et al. (2015) reported that chlorogenic acid could react with ε-amino groups of lysine side chain in lactoferrin, and the content of free amino group was decreased by 40.32 % after the reaction. Since 1 % SDS was added to destroy non-covalent bonds (Kroll, Rawel, & Rohn, 2003), the reduce in free amino content can be related to the covalent complexation between EGCG and LF.

The amount of free sulfhydryl group in LF-EGCG (3.39 μmol/g) was obviously lower than that of LF (1.58 μmol/g) ($p < 0.05$). The addition of 8 mol/L urea could inhibit free sulfhydryl groups to form disulfide bonds, so the decrease of free sulfhydryl group amount demonstrated EGCG covalently bound to the free sulfhydryl groups of LF. Therefore, the covalent bonds C—N and C—S were formed between the phenol rings of EGCG and the amino acids of LF under alkali treatment.

3.1.3. Changes in molecular weight

MALDI-TOF-MS was adopted to accurately detect the molecular weight changes of samples. From Fig. 1A, compared with LF, the molecular weight of LF-EGCG was higher and the peak became wider, while that of LF + EGCG had little change. After covalent binding, the changes in molecular weight indicated that at least four EGCG molecules were embedded in one LF molecule. The weak non-covalent interaction could be easily destroyed by acceleration voltage, flight distance, and electromagnetic field of MALDI-TOF-MS whereas the strong covalent bonds were not subject to these conditions (Wei et al., 2015). Hence, the raise of molecular weight suggested the formation of covalent bonds between EGCG and LF.

3.1.4. FTIR analysis

FTIR spectroscopy is usually applied to characterize the changes in molecular structure. As displayed in Fig. 1B, three main peaks were observed in LF: 3200–3500 cm^{-1} (amide A band, attributed to N—H stretching vibration and hydrogen bond vibration), 1654 cm^{-1} (amide I band, C═O stretching vibration) and 1541 cm^{-1} (amide II band, corresponded to C—H stretching and N—H bending mode) (Liu, Sun, Yang, et al., 2015). Compared with LF, blue shift occurred of amide A and amide II bands in LF + EGCG, which was related to non-covalent interactions between LF and EGCG. The shift of amide A and amide II bands in LF-EGCG demonstrated that $-NH_2$ in LF participated in the reaction. In addition, peaks at 1691 cm^{-1} and 1620 cm^{-1} in EGCG were ascribed to carbonyl stretching, and the characteristic peaks of 3479 cm^{-1} and 3355 cm^{-1} were caused by stretching vibration of phenol hydroxyl group, which were absent in both LF-EGCG and LF + EGCG, implying the phenol hydroxyl group and carbonyl group in EGCG reacted with LF. The FTIR spectra of LF-EGCG and LF + EGCG were very similar to LF, indicating LF was the main component of complexes. This

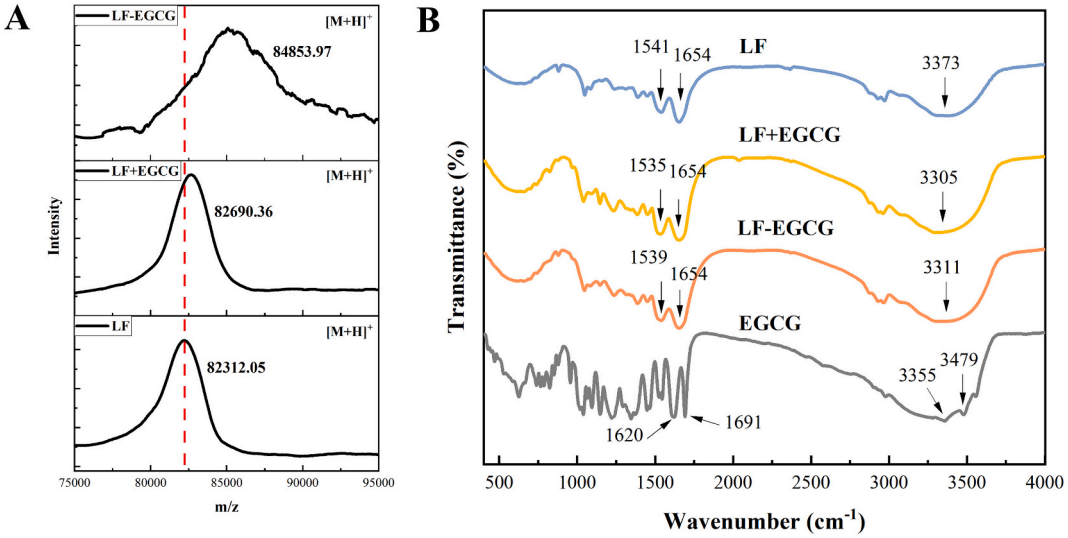

Fig. 1. MOLDI-TOF-MS spectra (A) and FTIR spectra (B) of LF, LF + EGCG, and LF-EGCG particles.

result was in agreement with the previous research (Li et al., 2021).

3.1.5. CD analysis

As shown in Fig. 2A∼B, the far-UV region (190–260 nm) of CD represented the secondary structure of samples, and the Near-UV CD region (250–320 nm) referred to the tertiary structure of samples. Redshift occurred in LF + EGCG and LF-EGCG spectra, and the peak intensity changed, manifesting the secondary structure of LF altered after covalent and non-covalent interactions with EGCG (Wei et al., 2015; Wu, Zhang, Kong, & Hua, 2009).

Compared with LF, the content of α-helix in LF + EGCG was raised, whereas the contents of β-sheet, β-turn and unordered were reduced (Fig. 2A). Studies had shown that the structure of α-helix was more compact and stable than β-sheet (Liu, Ru, & Ding, 2012; Yang, Xu, Liu, Yuan, & Gao, 2014), so the secondary structure of LF became more stable after non-covalent combination. The addition of EGCG introduced more -OH and increased the hydrogen bond interaction between them. Since the secondary structure of proteins was mainly maintained by hydrogen bonds, the unordered content decreased after non-covalent complexation. The contents of α-helix and β-turn were reduced while those of β-sheet and unordered were elevated after covalent binding, suggesting the secondary structure of LF was deconstructed, the firmness was decreased and the flexibility was increased (Li et al., 2021).

The near-UV spectra (250–320 nm) showed the molar ellipticity of complexes was significantly decreased compared with LF, and the impact of non-covalent interaction on tertiary structure was greater than that of covalent interaction, manifesting the tertiary structure of LF was significantly changed. Furthermore, Wei et al. (2015) reached similar conclusion in the combination of β-lactoglobulin with EGCG.

3.1.6. Fluorescence spectroscopy analysis

Proteins have intrinsic fluorescence, which is produced by aromatic amino acid residues (tyrosine, phenylalanine, tryptophan) (Liu, Sun, Wang, et al., 2015; Wu, Wu, & Hua, 2010). After the interaction between LF and small molecules, the emission peak was blue shifted when the protein conformation contraction made the tryptophan residue further located inside LF, and red-shifted when the protein conformation unfolding made the tryptophan residue further exposed from inside LF to the surface (Yang et al., 2015). Compared with LF, the fluorescence intensity of LF + EGCG was reduced and the absorption spectrum was redshifted (Fig. 2C), implying the protein structure was stretched and more tryptophan residues were exposed to react with EGCG. The fluorescence intensity of LF-EGCG was very low, and it was difficult to determine the peak of its emission wavelength, showing the interaction between EGCG and aromatic amino acids led to quenching of tryptophan fluorescence intensity. Therefore, the interaction between LF and EGCG caused irreversible changes in LF structure, more side chains exposed to the solution, and tryptophan was transferred to a more hydrophilic environment (Yang, Liu, Xu, Yuan, & Gao, 2014).

Three-dimensional fluorescence can provide more details of protein structure. From Fig. 2E, LF and its complexes had two peaks, peak a (represented Rayleigh scattering) and peak b (represented tyrosine residues and tryptophan residues) (Zhang et al., 2023). The order of fluorescence intensity of peak b was LF > LF + EGCG > LF-EGCG. This phenomenon showed EGCG quenched the endogenous fluorescence of LF, and the impact of covalent treatment on the endogenous fluorescence was greater than that of non-covalent treatment. Additionally, the E_m of LF + EGCG and LF-EGCG were redshifted by 4 nm and 5 nm, respectively. These changes indicated that the structure of LF was unfolding, being exposed to the solvent to a large extent. Meanwhile, the microenvironment of amino acid residues was changed, which was consistent with the results of fluorescence spectrum (Zhang, Zhou, et al., 2023; Zhao, Lin, Gao, Gong, & Mao, 2022).

3.1.7. Thermal stability

DSC spectra showed that LF had a single denaturation peak (81.92 °C). Research showed the denaturation temperature was relevant to iron saturation and the existing form of LF (Bokkhim, Bansal, GrØndahl, & Bhandari, 2013). Compared with LF, the denaturation temperature of LF-EGCG had no significant change while that of LF + EGCG was decreased from 81.92 °C to 74.36 °C (Fig. 2D). The higher the denaturation temperature, the denser the tertiary conformation of the protein and the higher the thermal stability (Feng, Wu, Wang, & Liu, 2016). Therefore, the tertiary and ordered structure of LF + EGCG were destroyed, which was corresponded with the above fluorescence results. Regarding the insignificant temperature change of LF-EGCG, further discussion remained.

3.1.8. Antioxidant activities

As seen in Fig. 2F∼G, the DPPH radical scavenging activity of LF was 4.52 %, whereas that of LF + EGCG and LF-EGCG was 51.55 % and 61.68 %, respectively. The ABTS radical activity of complexes was 1.33–1.87 times that of LF. The reducing power of complexes was increased by 137.64–354.40 μg V_c/mg sample compared with LF. The results demonstrated the antioxidant capacity of single protein was very low, but it was significantly improved when combined with polyphenols. Meanwhile, the antioxidant activity of LF-EGCG was stronger than LF + EGCG at the same concentration. It was associated with the higher polyphenol binding equivalent in LF-EGCG (Liu, Ma, Gao, & McClements, 2017). Therefore, LF-EGCG may be a potential antioxidant and antibacterial agent that can extend the shelf life of food.

3.1.9. Cytotoxicity

The covalent grafting of EGCG and LF may produce some toxic by-products while improving the antioxidant activity of LF. Therefore, it is necessary to estimate the toxicity of complexes prior to its application as an emulsifier in food processing. The effects of samples on Caco-2 cell viability were measured by MTT assay (Fig. 3). All samples showed no cytotoxicity within 12.5–200 μg/mL, and the cell survival rate was more than 90 %. With the increase of LF concentration, cell viability decreased slightly, but still remained at around 90 %. Overall, these particles were non-toxic and had certain biocompatibility in the range of 0–200 μg/mL.

3.1.10. Microstructure

AFM was applied to obtain the morphology changes in samples (Fig. 4A). In AFM images, the brighter the color, the higher the height. The images showed that LF was mainly spherical particles with a uniform surface. EGCG altered the size and morphology of LF, and the surface of complexes became irregular. The average roughness R_q values of LF-EGCG and LF + EGCG increased by 0.33 nm and 0.70 nm, respectively. After complexing with EGCG, the protein height increased and aggregation occurred. It was because that EGCG acted as a bridge between LF molecules and promoted their cross-linking, causing the formation of protein oligomers (Djuardi, Yuliana, Ogawa, Akazawa, & Suhartono, 2020). Furthermore, the height ranges in LF, LF + EGCG, and LF-EGCG were 4.5, 8.9, and 9.7 nm, respectively. Therefore, the modified proteins were more resistant to collapse than control protein (Li et al., 2021).

3.1.11. Wettability

The near-90° $\theta_{o/w}$ of particles promoted their effective adsorption and accumulation on the interface, forming steric hindrance to prevent droplets aggregation and improve the stability of emulsions (Jun et al., 2011). As exhibited in Fig. 4B, LF had a $\theta_{o/w}$ value of 95.3°. After non-covalent modification, the $\theta_{o/w}$ value of LF + EGCG was 103.5°. The poor wettability was caused by the exposure of hydrophobic groups in LF. The $\theta_{o/w}$ value of LF-EGCG was 87.5°, indicating LF-EGCG had greater potential to stabilize O/W Pickering emulsions. This result was also confirmed by the oil leakage in HIPPEs (Fig. 5A). Additionally, Dai et al. (2019) verified zein-propylene glycol alginate-rhamnolipid complex with neutral wettability could stabilize HIPPEs with good

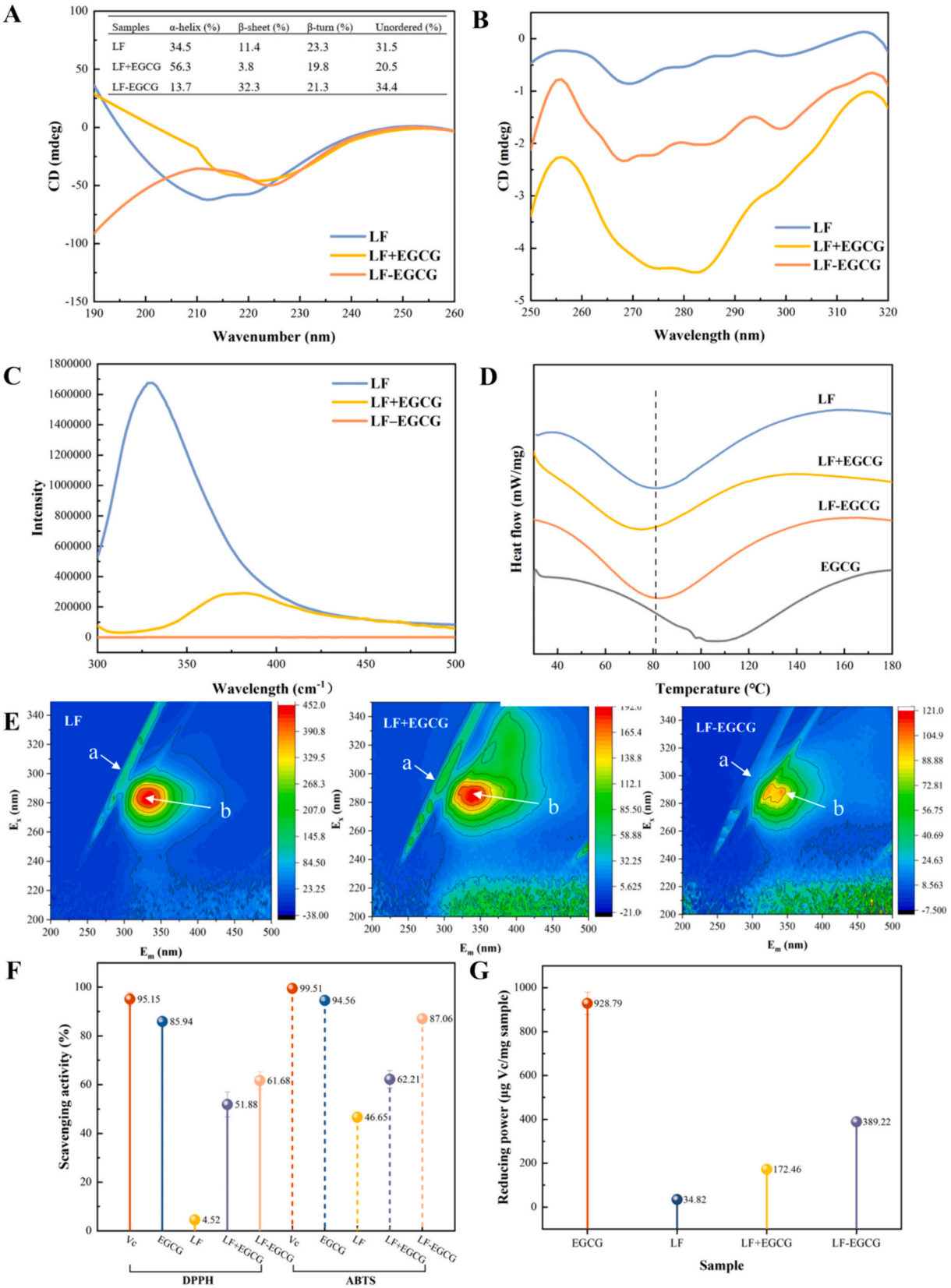

Fig. 2. The CD spectra (A ~ B), fluorescence spectra (C), DSC curves (D), three-dimensional fluorescence spectra (E), DPPH and ABTS radical scavenging activity (F), and reducing power (G) of LF, LF + EGCG, and LF-EGCG particles.

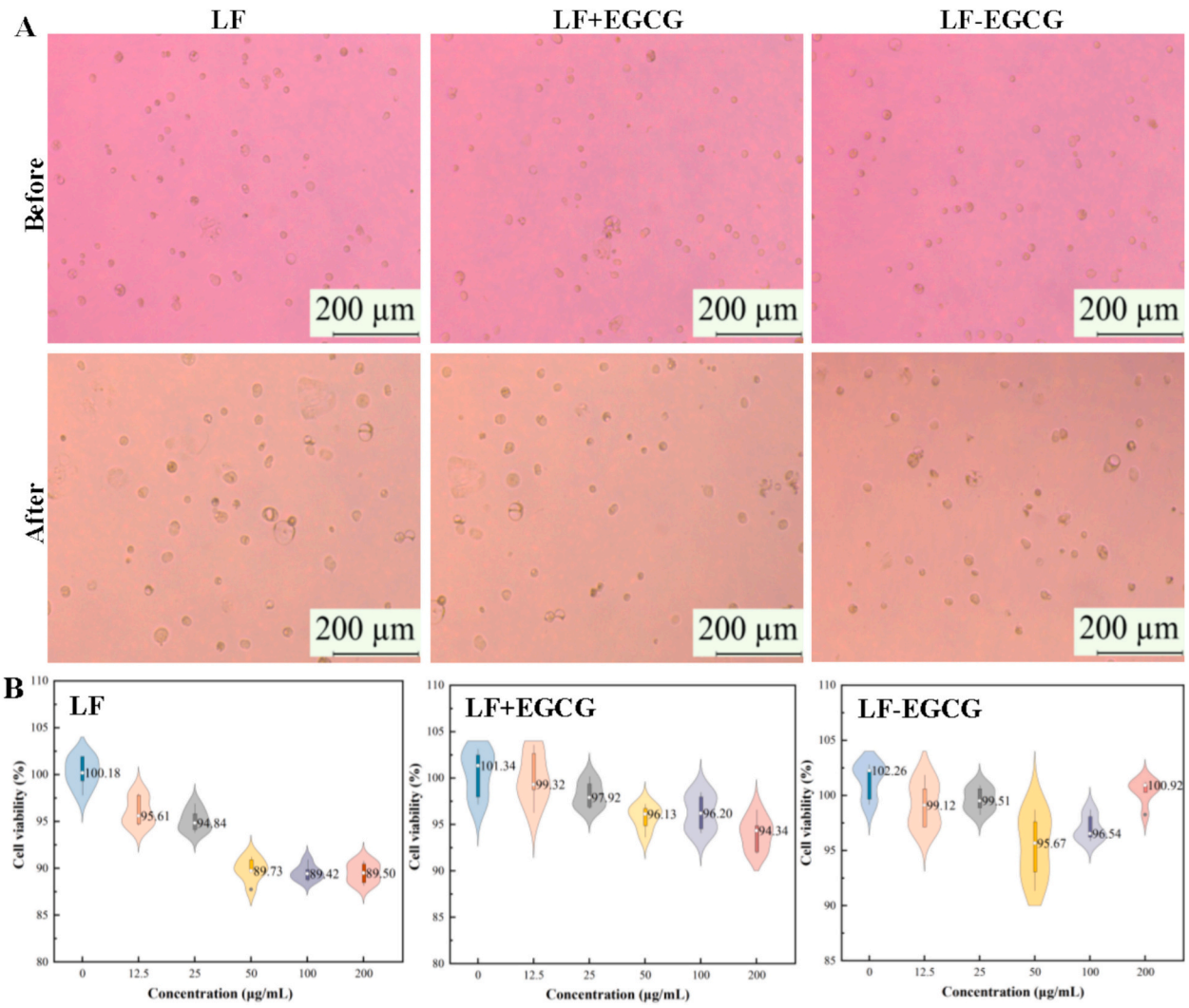

Fig. 3. Cell morphology before and after adding 200 μg/mL of protein solutions (A); cell viability of sample solutions at 0–200 μg/mL (B).

environmental stability.

3.1.12. *Particle size and ζ-potential analysis*

The particle size and ζ-potential of proteins varying with pH 3.0–10.0 were determined to assess the effect of pH on the stability of particles (Fig. 4D~E). The LF solution has a high positive charge at a low pH value and a high negative charge at a high pH value, and the isoelectric point (pI) appeared at pH 8.0–9.0. After binding with EGCG, the pI of LF-EGCG decreased to pH 5.0–6.0, while that of LF + EGCG changed to pH 7.0–8.0 (Fig. 4E). The results indicated EGCG could decrease pI after binding to proteins, which was in line with previous conclusion (Liu et al., 2016; Rawel, Rohn, & Kroll, 2003). Additionally, the absolute ζ-potential in LF-EGCG were the largest, so there was strong electrostatic repulsion among the particles (Zou et al., 2015).

The particle size of LF was increased after covalent and non-covalent complexation with EGCG. Near the pI, all protein particles had the largest particle size, and large aggregates appeared (Fig. 4D). As exhibited in Fig. 4C, LF + EGCG solutions were most turbidity among the three solutions, and significant aggregates appeared at pH 8–10. This phenomenon was consistent with ζ-potential measurement. The least net charge resulted in the least electrostatic repulsion among the particles within the pH range (Liu et al., 2016).

3.2. *Characterization of HIPPEs*

3.2.1. *Droplet size and ζ potential*

To obtain more stable HIPPEs, we explored the impacts of particle concentration on the formation of HIPPEs. From the appearance (Fig. 5A), all three particles can stabilize HIPPEs and did not flow when inverted. The emulsions were more stable with particle concentration increasing. However, 1.5 % (*w/v*) of LF and LF + EGCG HIPPEs were not stable and a small amount of oil separated on the surface of HIPPEs. In addition, LF + EGCG HIPPEs precipitated more oil than LF HIPPEs. The appearance of LF-EGCG HIPPEs was relatively stable throughout the concentration range except for 0.3 %. The drop size ($D_{4,3}$), size distribution and ζ-potential of emulsions were illustrated in Fig. 5B~C. As shown in Fig. 5B, $D_{4,3}$ of HIPPEs was decreased as the particle concentration increased. It could be explained by the fact that more particles were adsorbed to the interface, contributing to stabilizing larger interface and forming smaller droplets (Liu et al., 2023). Among the HIPPEs, the $D_{4,3}$ of LF-EGCG HIPPEs was lowest, indicating LF-EGCG may have the best emulsification property.

According to ζ-potential measurements (Fig. 5C), LF and LF + EGCG were positively charged while LF-EGCG was negatively charged. Initially, the emulsion was negatively charged (c = 0.3 %). As the concentration increased, the oil droplets were gradually coated by charged particles, so the emulsion had more and more positive or negative charges. Consequently, the enhance of electrostatic repulsion among the

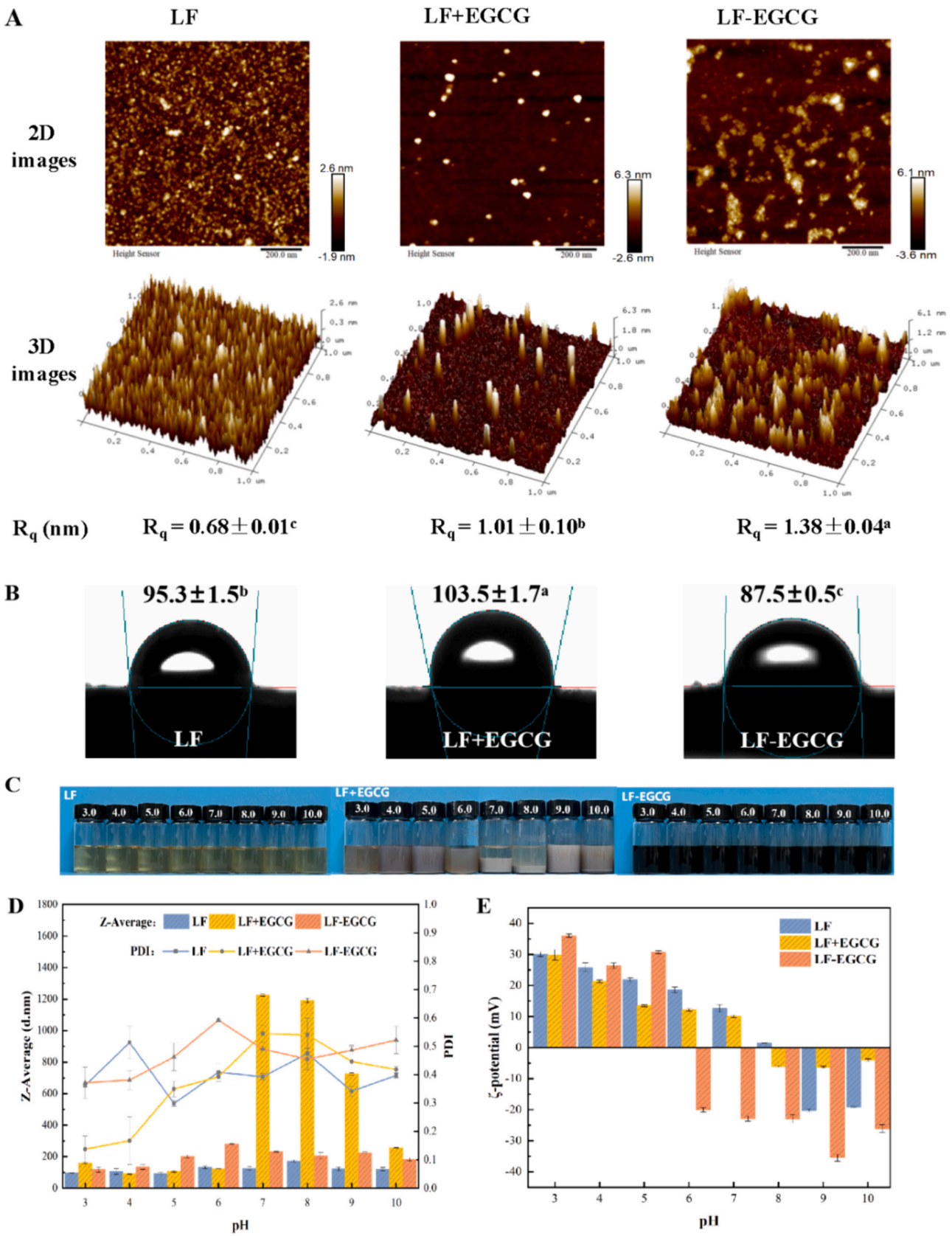

Fig. 4. AFM images (A), contact angle (B) of different samples; appearance (C), particle size (D) and ζ-potential (E) of LF, LF + EGCG, and LF-EGCG particles at pH 3.0–10.0. Different lowercase letters in the same figure indicated a statistically significant difference ($p < 0.05$).

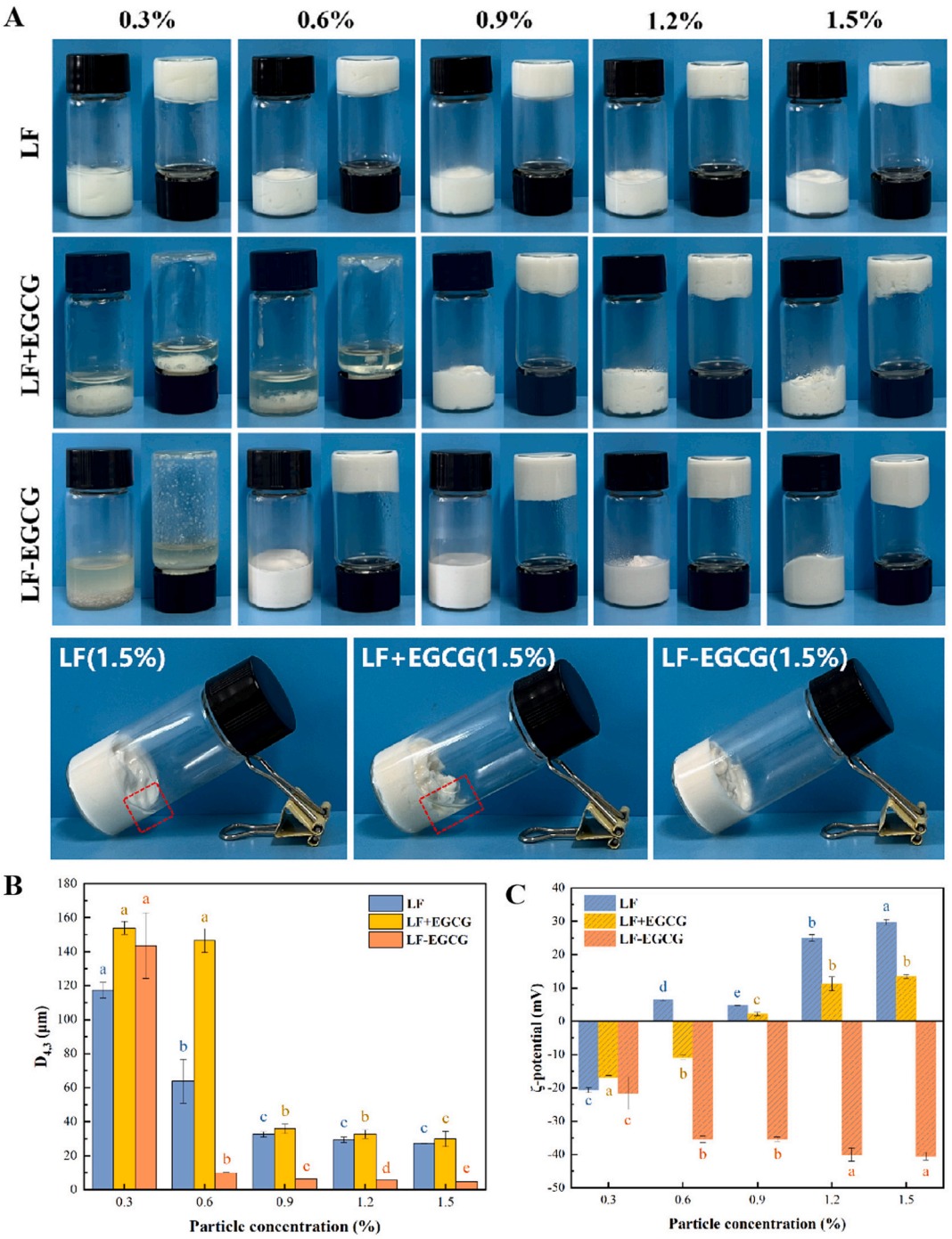

Fig. 5. Appearance (A), average droplet size ($D_{4,3}$) (B), and ζ-potential (C) of emulsions at different concentrations (0.3–1.5 %). Different lowercase letters in the same figure indicated a statistically significant difference ($p < 0.05$).

droplets might be another reason for the reduction of aggregation and $D_{4,3}$ (Ma et al., 2020). It was speculated that more oil leakage in LF + EGCG HIPPE may be due to the worst wettability and the least charge it carried. Below we focused on the HIPPEs stabilized by LF and LF-EGCG.

3.2.2. Microstructure analysis

The microstructure of HIPPEs was showed in Fig. 6. The green fluorescence (oil phase) was coated with red fluorescence (water phase), demonstrating the formation of O/W HIPPEs. Obviously, oil droplets in LF HIPPE were larger and uneven, but LF-EGCG HIPPE possessed more uniform droplet distribution and smaller droplet size. The result was corresponded to the data of droplet size, proving that covalent modification improved the stability of HIPPEs. The protein formed a denser interfacial film on the interface, preventing droplets from aggregating (Zhao, Fan, Zhou, & Li, 2023). Similar phenomenon was observed in zein-tannic acid stabilized emulsions (Liu et al., 2023).

3.2.3. LF-NMR and MRI analysis

LF-NMR was applied to reflect the water/oil distribution and physical state of HIPPEs. As illustrated in Fig. 6B, three characteristic peaks in T_2 relaxation time distribution were observed for each sample. T_{21} (1–10 ms) represented the water/oil molecules that firmly combined or intensely interacted with protein molecules in HIPPEs. T_{22} (20–130 ms) and T_{23} (130–1000 ms) were the limited mobile water/oil molecules

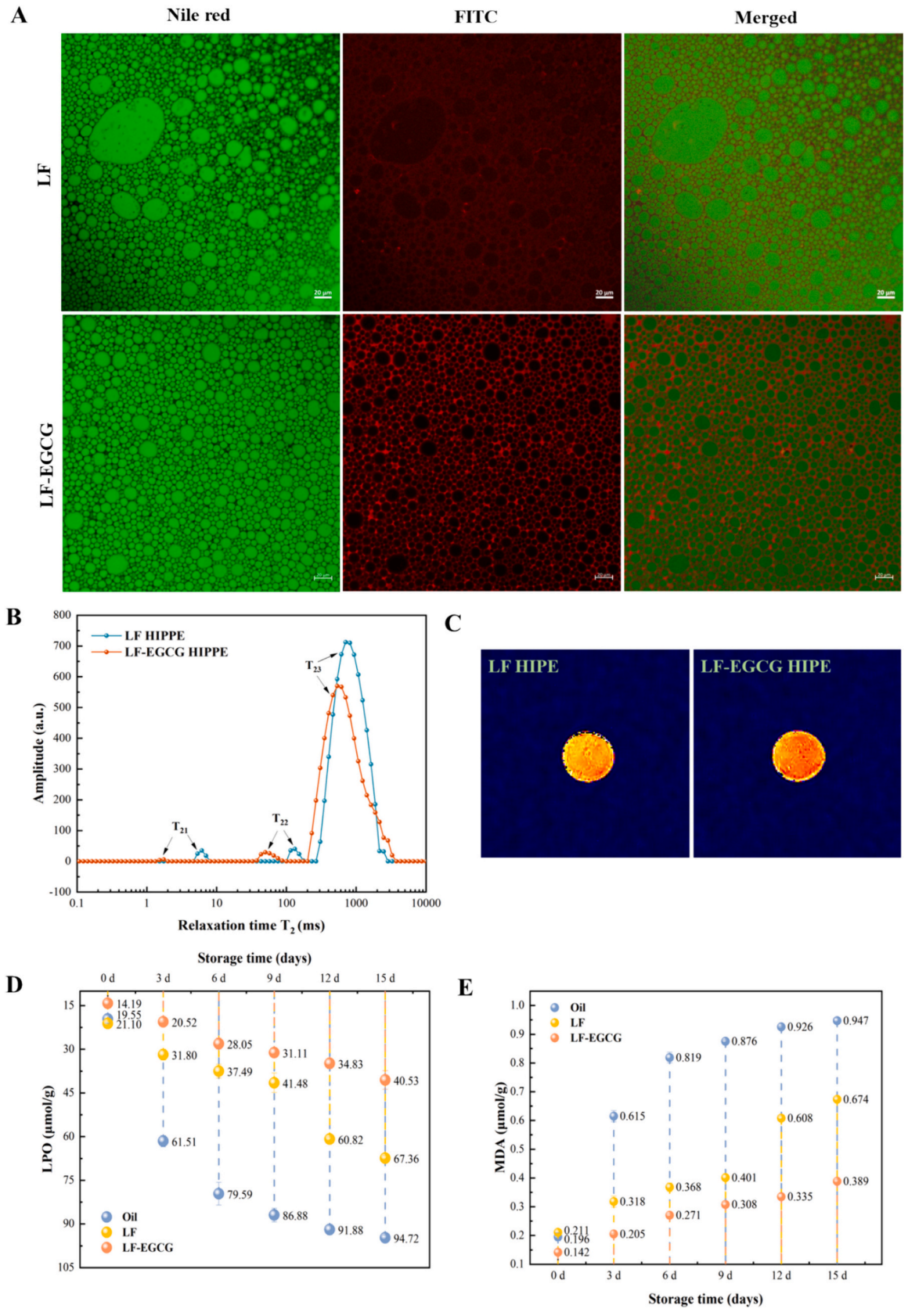

Fig. 6. CLSM images, scale bar: 20 μm (A); T_2 relaxation time distribution (B); MRI (C); LPO (D); and MDA (E) of HIPPEs stabilized with LF and LF-EGCG.

anchored in the organized gel network structure (Wang et al., 2024a). The proportions of T_{22} and T_{23} in both HIPPEs were above 95 %, showing the water/oil movement in HIPPEs was inhibited. The reduction of relaxation time in LF-EGCG HIPPE was relevant to the closer packing of smaller droplets, which hindered the motion of oil/water molecules (Yang et al., 2022). Therefore, the covalent modification improved the interaction of LF with water/oil.

Fig. 6C showed the oil/water proton MRI images of HIPPEs. The higher the signal intensity, the redder the image, which represented the moisture distribution in sampkes was more evenly. In contrast, blue represented uneven moisture distribution (Cheng et al., 2024). Compared with LF HIPPE, the red signal of LF-EGCG HIPPE was enhanced and more evenly distributed. This phenomenon demonstrated that the oil/water distribution in LF-EGCG HIPPE was more uniform and orderly. That is to say, a denser network structure was formed, which inhibited the aggregation of oil droplets. Similar result was also reported

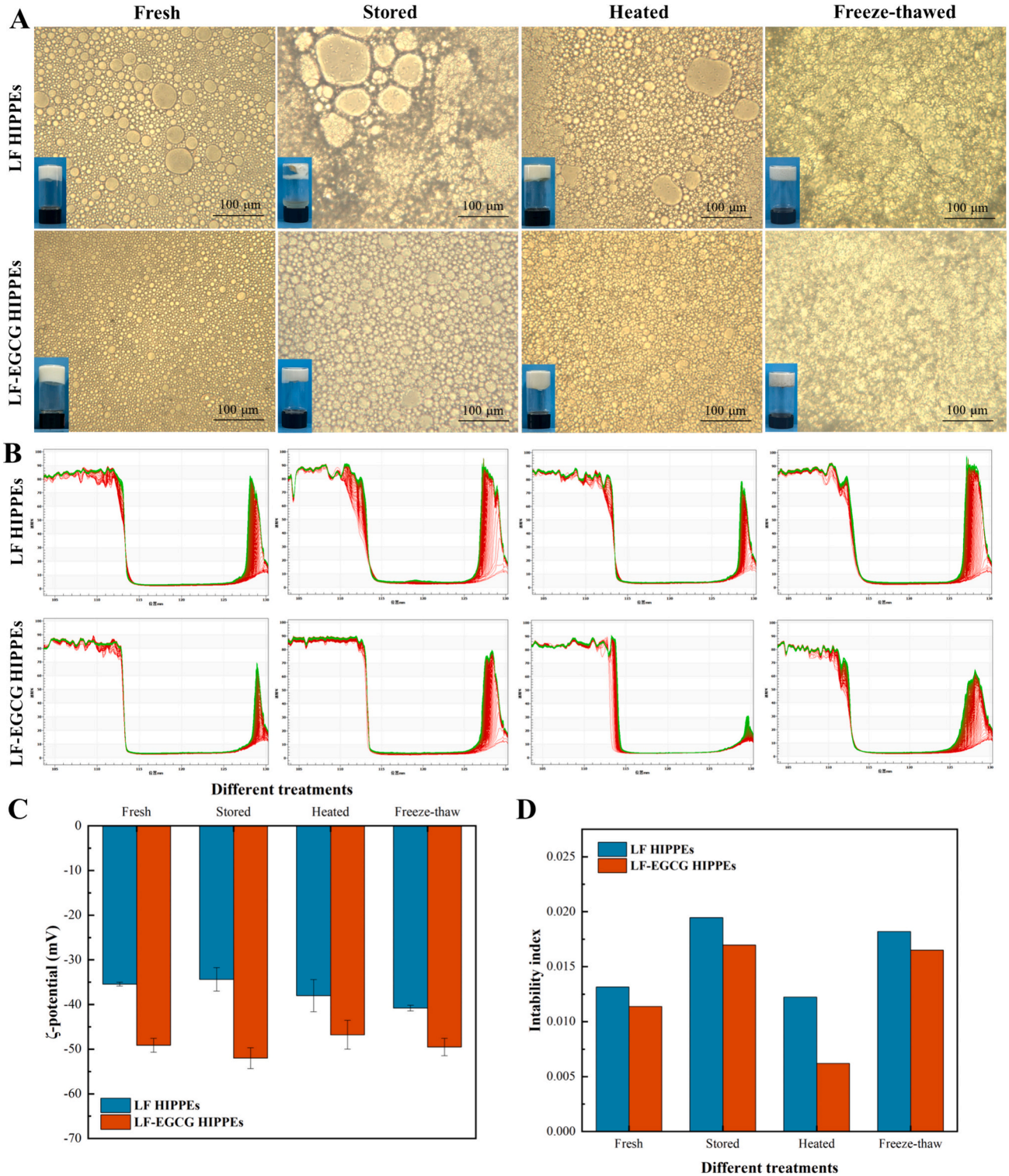

Fig. 7. Optical micrographs and visual appearance (A), physical stability (B), ζ-potential (C), and instability index (D) of HIPPEs stabilized with LF and LF-EGCG.

in the HIPPEs stabilized by pea protein isolate/mung bean starch complex (Li et al., 2024).

3.2.4. Lipid oxidation analysis

As seen in Fig. 6D∼E, after storing for 15 days, LPO content in fish oil was increased from 19.55 ± 1.43 μmol/g to 94.72 ± 0.91 μmol/g, while that of LF HIPPE and LF-EGCG HIPPE gradually increased to 67.36 ± 0.77 μmol/g and 40.53 ± 3.18 μmol/g, respectively. The MDA content of LF HIPPE and LF-EGCG HIPPE decreased by 29.47 % and 58.95 % compared with that of fish oil. Therefore, compared with the blank fish oil, the production of LPO and MDA in HIPPEs was inhibited. LF-EGCG complex exhibited stronger inhibition of lipid oxidation in the HIPPE, which was similar to the results of Feng et al. (Feng et al., 2018). This phenomenon was connected with the formation of particle-based oil-water interface film. A denser and stronger interface film acted as a physical barrier that shielded the interaction of unsaturated fatty acids and hydroperoxides with transition metals (Zhao et al., 2021). In addition, LF-EGCG acted as an antioxidant that scavenged free radicals and inhibited the formation of peroxides, thereby further improving the oxidation stability of HIPPEs.

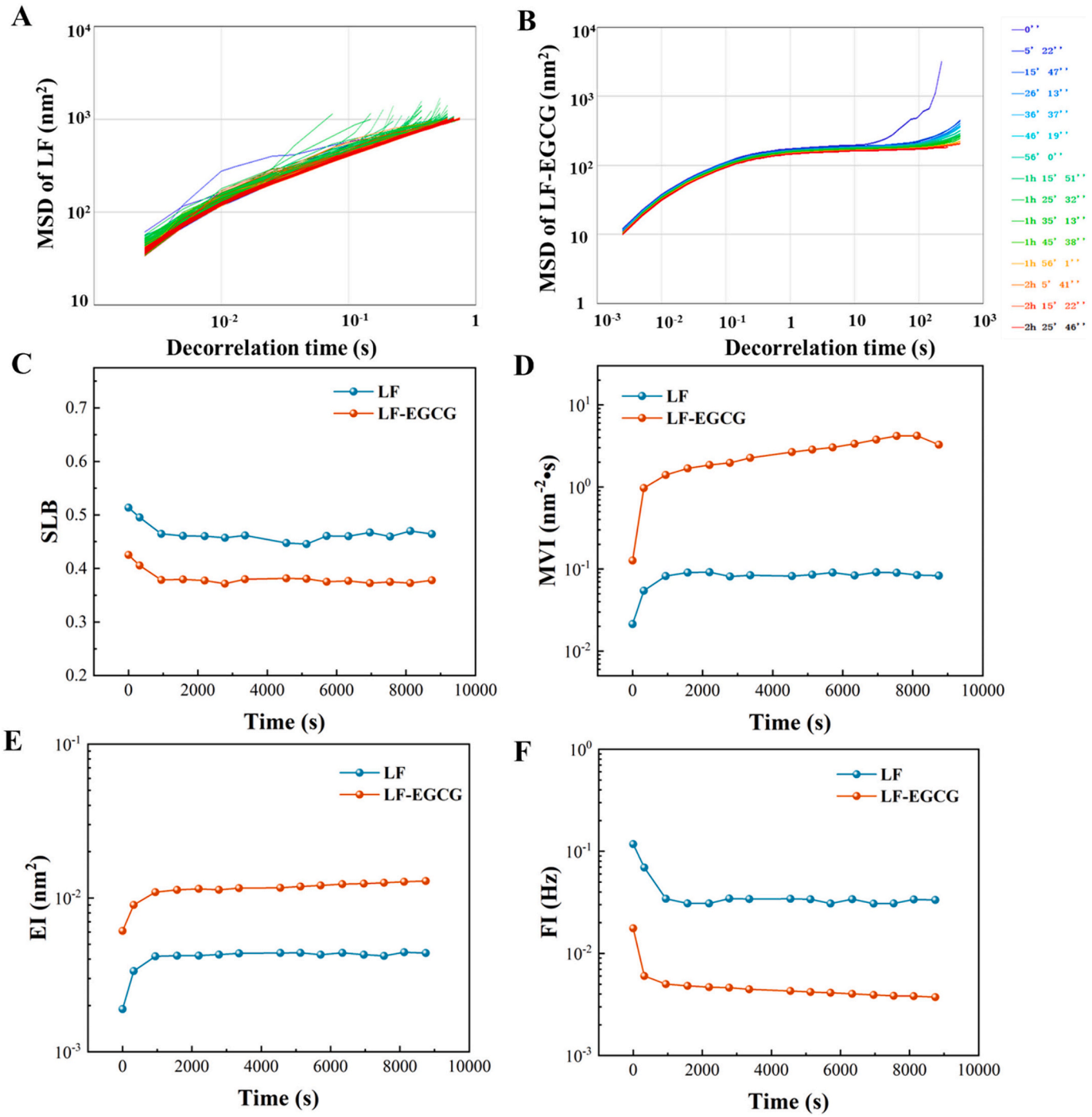

Fig. 8. The microrheological behavior of HIPPEs stabilized with LF and LF-EGCG: The changes of MSD (A ∼ B), SLB (C), MVI (D), EI (E), and FI (F) of HIPPEs during the tracking time.

3.2.5. Stability of HIPPEs

Since the prepared fish oil HIPPEs will be applied to food systems, it is very important to evaluate the physical, thermal, freeze-thaw, and storage stability of HIPPEs. As exhibited in Fig. 7A, compared with freshly prepared LF HIPPE, the oil droplets of freshly prepared LF-EGCG HIPPE were smaller and more uniform. The oil droplets in LF-EGCG HIPPEs were tightly packed and formed a denser network structure. After storage at 4 °C for 3 months, LF HIPPE showed obvious phase separation, while LF-EGCG HIPPE showed a good solid appearance and did not flow after inversion. The microstructure showed that the droplet size of both emulsions increased after storage. The microstructure of LF HIPPE was collapsed, and large droplets were appeared, while the droplets of LF-EGCG HIPPE was denser and more orderly, indicating that the storage stability of the emulsions was improved after covalent modification. After thermal and freeze-thaw treatments, both emulsions did not flow when inverted. The droplet structure of LF-EGCG HIPPEs was more stable, showing that LF-EGCG HIPPEs had an interfacial film with higher mechanical strength, which inhibited the damage of high temperature and ice crystals to their structure (Wang et al., 2024b). Fig. 7C showed the ζ-potential of HIPPEs did not change significantly after different treatments, but the ζ-potential of LF-EGCG HIPPEs was always higher than that of LF HIPPEs, which could better inhibit droplet aggregation.

The physical stability of HIPPEs was measured to simulate the effects of various physical forces on food during the process. The greater the change in the transmittance fluctuation curve over time, the higher the instability index, indicating the sample was more unstable. The fluctuation curve area and instability index of LF-EGCG HIPPEs were always lower than those of LF HIPPEs, which was consistent with the results of droplet size and ζ-potential. Interestingly, the physical stability of HIPPEs was increased after thermal treatment, suggesting that the protein molecules inside HIPPEs were denatured, forming macromolecular aggregates and even gelling (Wan et al., 2024). In addition, the enhanced interfacial layer and viscoelastic network structure of LF-EGCG HIPPEs restricted the movement of droplets, thus having better physical stability.

3.2.6. Microrheology

Different from shear rheology, DWS microrheometer obtained the viscoelasticity of HIPPEs by monitoring Brownian motion of particles without destroying the HIPPEs structure (Zou et al., 2015). The microrheological behavior curves were showed in Fig. 8. MSD curves of HIPPEs were not linear (Fig. 8A), implying that the HIPPEs had viscoelastic and typical shear thinning behaviors (Xu et al., 2018). The MSD curves of HIPPEs had three stages: linear stage (first stage, related to the viscosity of protein particles), plateau stage (second stage, representing the elasticity of HIPPEs), and rise stage (last stage, reflecting the macroscopic viscosity of HIPPEs). Compared with LF HIPPE, LF-EGCG HIPPE had a lower plateau value, which represented better elasticity (Nowicki et al., 2022). A higher rise stage in LF HIPPE implied that its droplets had lower macroscopic viscosity and higher fluidity (Tao et al., 2024).

SLB values reflected the solid-like or liquid-like property of samples (Yue, Huang, Zhu, Huang, & Huang, 2022). As seen in Fig. 8C, the SLB values of both HIPPEs were less than 0.5, which meant the HIPPEs were solid-like. The SLB value of LF-EGCG HIPPE was lower than that of LF HIPPE, that is, the structure of LF-EGCG HIPPE was more solid-like. It was due to LF-EGCG HIPPE had denser gel network structure. MVI was corresponded to the macroscopic viscosity of systems. The covalent treatment improved the macroscopic viscosity of HIPPE (Fig. 8D). It can be seen the EI value of the HIPPE was also increased after covalent modification (Fig. 8E), manifesting the elasticity of HIPPE was enhanced. Compared with LF HIPPE, the MVI and EI values of LF-EGCG HIPPE were increased to 8.61 times and 2.89 times, respectively. The dramatic increase of EI and MVI in LF-EGCG HIPPE was generally ascribed to the enhanced resistance among droplets. This phenomenon could be explained by that the introduce of EGCG caused a tighter network structure and spatial rearrangement of droplets (Xu et al., 2016). FI corresponded to the fluidity of systems and showed a negative correlation with MVI (Zhu et al., 2020). Therefore, the higher viscosity of LF-EGCG HIPPE resulted in lower fluidity (Fig. 8F).

4. Conclusion

In conclusion, covalent complex fabricated by alkali treatment had higher polyphenol content, less α-helix but more β-sheet than non-covalent complex. EGCG-grafting reaction improved surface wettability and antioxidant activity of LF. The complexes showed no cytotoxicity within the range of 12.5–200 μg/mL. Meanwhile, LF-EGCG HIPPEs possessed smaller droplet size, higher ζ-potential, better lipid oxidative and environmental stress stability. These findings demonstrated that LF-EGCG HIPPEs may be a stable delivery system to embed and protect the beneficial lipids and bioactive substances from damage. Next, we will further explore the relationship between the interfacial properties of lactoferrin-polyphenol complexes and the macroscopic properties of emulsions.

CRediT authorship contribution statement

Ying Sun: Writing – original draft, Validation, Software, Methodology, Investigation, Formal analysis, Data curation. **Mantong Zhao:** Writing – original draft, Software, Methodology, Data curation. **Zhongyuan Liu:** Writing – review & editing, Supervision, Software, Methodology, Conceptualization. **Haohao Shi:** Writing – review & editing, Visualization, Supervision, Conceptualization. **Xueying Zhang:** Writing – review & editing, Supervision, Conceptualization. **Yongqiang Zhao:** Writing – review & editing, Supervision, Conceptualization. **Zhenhua Ma:** Writing – review & editing, Conceptualization. **Gang Yu:** Writing – review & editing, Supervision, Conceptualization. **Guanghua Xia:** Writing – review & editing, Visualization, Supervision, Resources, Project administration, Funding acquisition, Conceptualization. **Xuanri Shen:** Writing – review & editing, Supervision, Conceptualization.

Declaration of competing interest

The authors declare that they have no known competing financial interests or personal relationships that could have appeared to influence the work reported in this paper.

Data availability

No data was used for the research described in the article.

Acknowledgements

The research was supported by the Primary Research & Development Plan of Hainan Province (No: ZDYF2024XDNY188), the Project of Sanya Yazhou Bay Science and Technology City (No: SKJC-2023-01-001), and the Primary Research & Development Plan of Hainan Province (No: ZDYF2022XDNY335).

Appendix A. Supplementary data

Supplementary data to this article can be found online at https://doi.org/10.1016/j.fochx.2024.101836.

References

Beveridge, T., Toma, S. J., & Nakai, S. (1974). Deyermination of SH- and SS-groups in some food proteins using ellman's reagent. *Journal of Food Science, 39*(1), 49–51. https://doi.org/10.1111/j.1365-2621.1974.tb00984.x

Bokkhim, H., Bansal, N., GrØndahl, L., & Bhandari, B. (2013). Physico-chemical properties of different forms of bovine lactoferrin. *Food Chemistry, 141*(3), 3007–3013. https://doi.org/10.1016/j.foodchem.2013.05.139

Cheng, X., Wang, H., Wang, Z., Zhao, Q., Lou, M., Meng, F., & Jiang, L. (2024). Development and characteristics of emulsion gels with microwave-assisted ferulic acid covalently modified soy protein: Structure, function and digestive properties. *Food Hydrocolloids, 146*, Article 109230. https://doi.org/10.1016/j.foodhyd.2023.109230

Dai, L., Yang, S., Wei, Y., Sun, C., McClements, D. J., Mao, L., & Gao, Y. (2019). Development of stable high internal phase emulsions by Pickering stabilization: Utilization of zein-propylene glycol alginate-rhamnolipid complex particles as colloidal emulsifiers. *Food Chemistry, 275*, 246–254. https://doi.org/10.1016/j.foodchem.2018.09.122

Djuardi, A. U. P., Yuliana, N. D., Ogawa, M., Akazawa, T., & Suhartono, M. T. (2020). Emulsifying properties and antioxidant activity of soy protein isolate conjugated with tea polyphenol extracts. *Journal of Food Science and Technology, 57*(10), 3591–3600. https://doi.org/10.1007/s13197-020-04391-9

Feng, J., Cai, H., Wang, H., Li, C., & Liu, S. (2018). Improved oxidative stability of fish oil emulsion by grafted ovalbumin-catechin conjugates. *Food Chemistry, 241*, 60–69. https://doi.org/10.1016/j.foodchem.2017.08.055

Feng, J., Wu, S., Wang, H., & Liu, S. (2016). Improved bioavailability of curcumin in ovalbumin-dextran nanogels prepared by Maillard reaction. *Journal of Functional Foods, 27*, 55–68. https://doi.org/10.1016/j.jff.2016.09.002

Feng, S., Zhang, S., Jiang, M., Liu, F., Chen, K., & Zhang, Y. (2023). Effects of glycation methods on the interfacial behavior and emulsifying performance of soy protein isolate-gum Arabic conjugates. *International Journal of Biological Macromolecules, 233*, Article 123554. https://doi.org/10.1016/j.ijbiomac.2023.123554

Feng, T., Wang, X., Wang, X., Xia, S., & Huang, Q. (2021). Plant protein-based antioxidant Pickering emulsions and high internal phase Pickering emulsions against broad pH range and high ionic strength: Effects of interfacial rheology and microstructure. *LWT, 150*, Article 111953. https://doi.org/10.1016/j.lwt.2021.111953

Kroll, J., Rawel, H., & Rohn, S. (2003). Reactions of plant phenolics with food proteins and enzymes under special consideration of covalent bonds. *Food Science and Technology Research, 9*, 205–218. https://doi.org/10.3136/fstr.9.205

Li, S., Zhu, Y., Hao, X., Su, H., Chen, X., & Yao, Y. (2024). High internal phase Pickering emulsions stabilized by the complexes of ultrasound-treated pea protein isolate/mung bean starch for delivery of β-carotene. *Food Chemistry, 440*, Article 138201. https://doi.org/10.1016/j.foodchem.2023.138201

Li, X., Li, M., Zhang, T., McClements, D. J., Liu, X., Wu, X., & Liu, F. (2021). Enzymatic and nonenzymatic conjugates of lactoferrin and (−)-epigallocatechin gallate: Formation, structure, functionality, and allergenicity. *Journal of Agricultural and Food Chemistry, 69*(22), 6291–6302. https://doi.org/10.1021/acs.jafc.1c01167

Liu, F., Liang, X., Yan, J., Zhao, S., Li, S., Liu, X., & McClements, D. J. (2022). Tailoring the properties of double-crosslinked emulsion gels using structural design principles: Physical characteristics, stability, and delivery of lycopene. *Biomaterials, 280*, Article 121265. https://doi.org/10.1016/j.biomaterials.2021.121265

Liu, F., Ma, C., Gao, Y., & McClements, D. J. (2017). Food-grade covalent complexes and their application as nutraceutical delivery systems: A review. *Comprehensive Reviews in Food Science and Food Safety, 16*(1), 76–95. https://doi.org/10.1111/1541-4337.12229

Liu, F., Sun, C., Wang, D., Yuan, F., & Gao, Y. (2015). Glycosylation improves the functional characteristics of chlorogenic acid–lactoferrin conjugate. *RSC Advances, 5*(95), 78215–78228. https://doi.org/10.1039/C5RA15261E

Liu, F., Sun, C., Yang, W., Yuan, F., & Gao, Y. (2015). Structural characterization and functional evaluation of lactoferrin–polyphenol conjugates formed by free-radical graft copolymerization. *RSC Advances, 5*(20), 15641–15651. https://doi.org/10.1039/C4RA10802G

Liu, F., Wang, D., Sun, C., McClements, D. J., & Gao, Y. (2016). Utilization of interfacial engineering to improve physicochemical stability of β-carotene emulsions: Multilayer coatings formed using protein and protein–polyphenol conjugates. *Food Chemistry, 205*, 129–139. https://doi.org/10.1016/j.foodchem.2016.02.155

Liu, J., Ru, Q., & Ding, Y. (2012). Glycation a promising method for food protein modification: Physicochemical properties and structure, a review. *Food Research International, 49*(1), 170–183. https://doi.org/10.1016/j.foodres.2012.07.034

Liu, X., Xie, F., Zhou, J., He, J., Din, Z.-U., Cheng, S., & Cai, J. (2023). High internal phase Pickering emulsion stabilized by zein-tannic acid-sodium alginate complexes: β-carotene loading and 3D printing. *Food Hydrocolloids, 142*, Article 108762. https://doi.org/10.1016/j.foodhyd.2023.108762

Ma, L., Zou, L., McClements, D. J., & Liu, W. (2020). One-step preparation of high internal phase emulsions using natural edible Pickering stabilizers: Gliadin nanoparticles/gum Arabic. *Food Hydrocolloids, 100*, Article 105381. https://doi.org/10.1016/j.foodhyd.2019.105381

Nowicki, J., Woch, J., Drabik, J., Korasiak, K., Iłowska, J., & Osuch-Słomka, E. (2022). Formation, properties and rheology of paraffin wax oil-in-water emulsions. Stabilizing effect of novel EO/PO/EO block copolymer fatty acid monoesters. *Materials Chemistry and Physics, 291*, 126759. https://doi.org/10.1016/j.matchemphys.2022.126759

Rawel, H. M., Rohn, S., & Kroll, J. (2003). Influence of a sugar moiety (rhamnosylglucoside) at 3-O position on the reactivity of quercetin with whey proteins. *International Journal of Biological Macromolecules, 32*(3), 109–120. https://doi.org/10.1016/S0141-8130(03)00044-8

Song, Y., Zhou, L., Zhang, D., Wei, Y., Jiang, S., Chen, Y., & Shao, X. (2023). Stability and release of peach polyphenols encapsulated by Pickering high internal phase emulsions in vitro and in vivo. *Food Hydrocolloids, 139*, Article 108593. https://doi.org/10.1016/j.foodhyd.2023.108593

Tao, Y., Cai, J., Wang, P., Chen, J., Zhou, L., Yang, Z., & Xu, X. (2024). Exploring the relationship between the interfacial properties and emulsion properties of ultrasound-assisted cross-linked myofibrillar protein. *Food Hydrocolloids, 146*, 109287. https://doi.org/10.1016/j.foodhyd.2023.109287

Tong, Q., Yi, Z., Ran, Y., Chen, X., Chen, G., & Li, X. (2021). Green tea polyphenol-stabilized gel-like high internal phase Pickering emulsions. *ACS Sustainable Chemistry & Engineering, 9*(11), 4076–4090. https://doi.org/10.1021/acssuschemeng.0c08633

Wan, X., Kang, Q., Li, J., Guo, M., Li, P., Shi, H., & Xia, G. (2024). Effect of NaCl concentration on the formation of high internal phase emulsion based on whey protein isolate microgel particles. *Food Chemistry, 433*, Article 137395. https://doi.org/10.1016/j.foodchem.2023.137395

Wan, X., Zhao, M., Guo, M., Li, P., Shi, H., Zhang, X., & Xia, G. (2023). Characterization of coacervation behavior between whey protein isolate and gum Arabic: Effects of heat treatment. *Food Chemistry: X, 18*, Article 100703. https://doi.org/10.1016/j.fochx.2023.100703

Wang, L.-J., Yin, S.-W., Wu, L.-Y., Qi, J.-R., Guo, J., & Yang, X.-Q. (2016). Fabrication and characterization of Pickering emulsions and oil gels stabilized by highly charged zein/chitosan complex particles (ZCCPs). *Food Chemistry, 213*, 462–469. https://doi.org/10.1016/j.foodchem.2016.06.119

Wang, Y., Hu, D., Yue, W., You, J., Yin, T., Rong, J., & Hu, Y. (2024a). High internal phase emulsions of ω-3 fatty acids stabilized by fish scale gelatin particles: Application to lipid-enhanced surimi 3D printing. *Food Hydrocolloids, 146*, Article 109254. https://doi.org/10.1016/j.foodhyd.2023.109254

Wang, Y., Yang, Y., Xu, L., Qiu, C., Jiao, A., & Jin, Z. (2024b). Rheology and stability mechanism of pH-responsive high internal phase emulsion constructed gel by pea protein and hydroxypropyl starch. *Food Chemistry, 440*, Article 138233. https://doi.org/10.1016/j.foodchem.2023.138233

Wei, Z., Yang, W., Fan, R., Yuan, F., & Gao, Y. (2015). Evaluation of structural and functional properties of protein–EGCG complexes and their ability of stabilizing a model β-carotene emulsion. *Food Hydrocolloids, 45*, 337–350. https://doi.org/10.1016/j.foodhyd.2014.12.008

Wu, W., Wu, X., & Hua, Y. (2010). Structural modification of soy protein by the lipid peroxidation product acrolein. *LWT - Food Science and Technology, 43*(1), 133–140. https://doi.org/10.1016/j.lwt.2009.05.006

Wu, W., Zhang, C., Kong, X., & Hua, Y. (2009). Oxidative modification of soy protein by peroxyl radicals. *Food Chemistry, 116*(1), 295–301. https://doi.org/10.1016/j.foodchem.2009.02.049

Xu, Y., Tang, C., Liu, T., & Liu, R. (2018). Ovalbumin as an outstanding Pickering nanostabilizer for high internal phase emulsions. *Journal of Agricultural and Food Chemistry, 66*(33), 8795–8804. https://doi.org/10.1021/acs.jafc.8b02183

Yang, W., Liu, F., Xu, C., Sun, C., Yuan, F., & Gao, Y. (2015). Inhibition of the aggregation of lactoferrin and (−)-epigallocatechin gallate in the presence of polyphenols, oligosaccharides, and collagen peptide. *Journal of Agricultural and Food Chemistry, 63*(20), 5035–5045. https://doi.org/10.1021/acs.jafc.5b01881

Yang, W., Liu, F., Xu, C., Yuan, F., & Gao, Y. (2014). Molecular interaction between (−)-epigallocatechin-3-gallate and bovine lactoferrin using multi-spectroscopic method and isothermal titration calorimetry. *Food Research International, 64*, 141–149. https://doi.org/10.1016/j.foodres.2014.06.001

Yang, W., Xu, C., Liu, F., Yuan, F., & Gao, Y. (2014). Native and Thermally Modified Protein–Polyphenol Coassemblies: Lactoferrin-Based Nanoparticles and Submicrometer Particles as Protective Vehicles for (−)-Epigallocatechin-3-gallate. *Journal of Agricultural and Food Chemistry, 62*(44), 10816–10827. https://doi.org/10.1021/jf5038147

Yang, Y., Zhang, M., Li, J., Su, Y., Gu, L., Yang, Y., & Chang, C. (2022). Construction of egg white protein particle and rhamnolipid based emulsion gels with β-sitosterol as gelation factor: The application in cookie. *Food Hydrocolloids, 127*, Article 107479. https://doi.org/10.1016/j.foodhyd.2021.107479

Yıldırım, A., Mavi, A., & Kara, A. A. (2001). Determination of antioxidant and antimicrobial activities of Rumex crispus L. extracts. *Journal of Agricultural and Food Chemistry, 49*(8), 4083–4089. https://doi.org/10.1021/jf0103572

Zhang, F., Wang, P., Huang, M., & Xu, X. (2024). Modulating the properties of myofibrillar proteins-stabilized high internal phase emulsions using chitosan for enhanced 3D-printed foods. *Carbohydrate Polymers, 324*, Article 121540. https://doi.org/10.1016/j.carbpol.2023.121540

Zhang, L., Zhou, C., Xing, S., Chen, Y., Su, W., Wang, H., & Tan, M. (2023). Sea bass protein-polyphenol complex stabilized high internal phase of algal oil Pickering emulsions to stabilize astaxanthin for 3D food printing. *Food Chemistry, 417*, Article 135824. https://doi.org/10.1016/j.foodchem.2023.135824

Zhang, M., Fan, L., Liu, Y., & Li, J. (2023). Effects of alkali treatment on structural and functional properties of chickpea protein isolate and its interaction with gallic acid: To improve the physicochemical stability of water–in–oil emulsions. *Food Hydrocolloids, 140*, Article 108601. https://doi.org/10.1016/j.foodhyd.2023.108601

Zhang, Y., Xin, N., Ashaolu, T. J., Chen, N., Wang, Y., Zhang, T., & Zhao, C. (2023). In vitro and in silico studies of the structure and functional properties of the lactoferrin-chlorogenic acid complex. *Food Hydrocolloids, 144*, Article 109051. https://doi.org/10.1016/j.foodhyd.2023.109051

Zhao, J., Lin, W., Gao, J., Gong, H., & Mao, X. (2022). Limited hydrolysis as a strategy to improve the non-covalent interaction of epigallocatechin-3-gallate (EGCG) with whey protein isolate near the isoelectric point. *Food Research International, 161*, Article 111847. https://doi.org/10.1016/j.foodres.2022.111847

Zhao, Q., Fan, L., Zhou, Y., & Li, J. (2023). Effect of chitosan-protocatechuic acid conjugate on stability and encapsulation capacity of polysaccharide-based high

internal phase emulsion. *Carbohydrate Polymers, 304*, Article 120487. https://doi.org/10.1016/j.carbpol.2022.120487

Zhao, T., Huang, L., Luo, D., Xie, Y., Zhang, Y., Zhang, Y., & Zhao, M. (2021). Fabrication and characterization of anchovy protein hydrolysates-polyphenol conjugates with stabilizing effects on fish oil emulsion. *Food Chemistry, 351*, Article 129324. https://doi.org/10.1016/j.foodchem.2021.129324

Zou, Y., Guo, J., Yin, S., Wang, J., & Yang, X. (2015). Pickering emulsion gels prepared by hydrogen-bonded zein/tannic acid complex colloidal particles. *Journal of Agricultural and Food Chemistry, 63*(33), 7405–7414. https://doi.org/10.1021/acs.jafc.5b03113